Single Molecule Tracking Studies of Lower Critical Solution Temperature Transition Behavior in Poly(N-isopropylacrylamide)

Lindsay C.C. Elliott[1□], Moussa Barhoum[2□], Joel M. Harris[2] and Paul W. Bohn[3*]*

[1]Department of Chemistry, University of Illinois at Urbana-Champaign, 600 S. Mathews Ave., Urbana, IL 61801

[2]Department of Chemistry, University of Utah, 315 South 1400 East, Salt Lake City, UT 84112

[3]Department of Chemical and Biomolecular Engineering and Department of Chemistry and Biochemistry, University of Notre Dame, Notre Dame, IN 46556

[*]Authors to whom correspondence should be addressed: *pbohn@nd.edu, harrisj@chem.utah.edu.* [□]LCCE and MB contributed equally to this work.

Keywords: *Single molecule tracking, atom transfer radical polymerization, poly(N-isopropylacrylamide), stimulus responsive polymer, temperature sensitive hydrogel, free volume change, lower critical solution temperature, confinement level calculations, radius of gyration evolution, SMT, ATRP, pNIPAAm, SRP, LCST*

Abstract

Spatial and temporal heterogeneities in expanded and collapsed surface bound pNIPAAm films are studied by single molecule tracking (SMT) experiments. Tracking data are analyzed using both radius of gyration (R_g) evolution and confinement level calculations to elucidate the range of behaviors displayed by single Rhodamine6G (R6G) molecules. Confined diffusion that is dictated by the free volume within surface tethered chains is observed with considerable dispersion among individual R6G molecules. Thus, the distribution of probe behavior reflects nanometer scale information about the state of the polymer brush at temperatures above ($T > T_{LCST}$) and below ($T < T_{LCST}$) the lower critical solution temperature (LCST). In this context, confinement level analysis and R_g evolution both show a larger degree of confinement of the probe in pNIPAAm at $T > T_{LCST}$. Temperature-dependent changes in confinement are evidenced at $T > T_{LCST}$ by a higher percentage of confined steps, longer periods of confined events, and smaller area of confined zones as well as a shift in the overall distribution of R_g evolution paths and final R_g distributions.

Introduction

Stimulus-responsive materials (SRMs) have attracted enormous attention due to their ability to react to external stimuli by increasing or decreasing the free volume between individual polymer chains, resulting in the transport of water into or out of the material, thus producing changes in size or shape of polymer brushes consisting of these materials. Physical and chemical properties such as free volume, thickness, hydrophilicity, and charge state can all be controlled by modulating polymer density, degree of cross-linking, and chemical environment.[1-4] A variety of external stimuli, *e.g.* electric field, ionic strength and pH of the surrounding solution, analyte concentration, and light exposure, have been exploited to initiate shape/size/property transitions in different SRMs.[5-7]

One model SRM, poly(N-isopropylacrylamide), pNIPAAm, is a temperature responsive polymer that exhibits a lower critical solution temperature (LCST), at which a transition occurs - from an expanded hydrophilic form ($T < T_{LCST}$) to a collapsed, hydrophobic morphology ($T > T_{LCST}$).[8, 9] The LCST phenomenon in pNIPAAm is of great interest technologically due to its proximity to human body temperature. Thus, applications in controlled drug delivery have been widely studied, and although the phenomenology is controllable, the underlying physical and chemical behavior is found to be quite complex. Thus, the temporal and spatial heterogeneities exhibited in the temperature responsive polymer are particularly relevant to the loading and unloading of drug delivery devices. In addition, the ability to realize size and shape control on the nanometer length scale holds considerable promise for applications in tissue engineering, drug delivery systems, biosensors and actuators, and synthetic extracellular matrices.[10] However, at present, nanoscale SRM structures must be designed and tested empirically, since the behavior of SRMs is not understood well enough to support rational design with such fine

control. Detailed, molecular-level information is needed, which could be used to develop predictive models for stimulus-initiated molecular reorganization.

In order to examine the temperature-dependent behavior of SRMs on a single molecule level, the motions of fluorescent probes, Rhodamine6G (R6G), within surface-bound thin-films of pNIPAAm prepared by atom transfer radical polymerization (ATRP), are studied using single molecule tracking (SMT). SMT has become a viable research tool within the last two decades[11-17] after technological advances in collection device efficiency and in fluorophore quantum yield and lifetime. In SMT, the paths of intrinsic, inserted, or tagged probe molecules are tracked in order to gain information about position and mobility.[18] This technique has the advantage of interrogating the population of fluorophores on an individual basis, thus collecting and preserving spatial and temporal heterogeneities. SMT has been applied to various complex systems, such as hierarchical mobility in polymer networks,[19] molecular transport in thin silica sol-gel films,[20] membrane dynamics,[21] and pore dynamics within polyacrylamide gels.[22] Of particular interest in our laboratories is the use of SMT to understand the molecular-scale behavior of SRMs for use in actively controlled micro total analysis systems (μTAS).[23] Thus, SMT is a very attractive approach for real time investigation of spatial and temporal heterogeneities in the structure of soft materials undergoing molecular reorganization at or near the LCST. In addition to the specific temperature-responsive behavior of pNIPAAm studied here, the methodology can be extended to investigate the underlying basis for a wide range of soft material dynamic properties.

Experimental

Materials. Unless otherwise noted reagents and solvents were obtained from Sigma Aldrich., Rhodamine 6G (99%, Acros), 11-trichlorosilyundecyl-2'-bromo-2-isobutyrate (silane

initiator) (95+%, ATRP Solutions), hexanes (ACS reagent, 99.9%, Fisher), dichloromethane (DCM, Chromasol Plus), ethanol (EtOH, denatured for HPLC, Acros), isopropanol (IPA, ACS reagent, >99.5%), cuprous bromide (CuBr, 99.999%), ethanol (EtOH, 99%, Fisher), and dimethyl formamide (DMF, ACS reagent, >99.8%) were used as received. N-isopropylacrylamide (NIPAAm, 97%) was purified by running a 1:1 hexanes/DCM saturated solution through a 2.5 cm basic alumina column, removing the solvent by reduced pressure evaporation, recrystallizing the remaining solid in hot hexanes at < 50°C, rinsing with minimal ice cold hexanes, and removing the solvent by reduced pressure evaporation. Methanol (MeOH, ACS reagent, 99.9%, Fisher), pentamethyldiethylene-triamine (PMDETA, 99%) and deionized (DI, ρ = 18 MΩ cm, Millipore Corp.) water were degassed by bubbling argon for 5-10 minutes and immediately transferred into the glovebox.

Sample preparation. Synthetic methods are described in detail elsewhere;[24] a brief description is as follows. Samples of surface bound pNIPAAm brushes of 70 nm unhydrated thickness were prepared by: (1) cleaning the substrate (silicon or glass) with piranha solution; (2) forming a monolayer of silane initiator, 11-trichlorosilyundecyl-2′-bromo-2-isobutyrate, on a substrate for ATRP was accomplished by liquid deposition; and (3) growing polymer using an ATRP grafting-from approach starting with the initiator monolayer in the presence of N-isopropylacrylamide, CuBr and pentamethyldiethylenetriamine (PMDETA) in 30 mL of 1:1 v:v MeOH/water in an oxygen-free atmosphere. Immediately after growth polymer thickness was characterized with profilometry (Sloan Dektak^3 ST) and/or ellipsometry (Gaertner Variable Angle Stokes Ellipsometer L116S). Single fluorescent R6G molecules, used as the fluorescent probe, were partitioned into pNIPAAm film target media by immersion of the film in DI H_2O

followed by addition of 1 nM R6G in methanol until a final concentration of 3.3 pM was reached. After partitioning, the film was imaged immediately.

Temperature-controlled ellipsometry. A custom built cell with polystyrene windows at 70° angles (normal to the incident and reflected laser light) was used to collect ellipsometry data. The aluminum floor of the cell was glued with silver epoxy to an aluminum disc that was fitted with a temperature collar (Bioptechs) with 0.1°C resolution capable of producing temperatures in the range ~19°C < T < 43°C depending on ambient room temperature. The polymer on silicon sample was placed inside the cell and immersed in DI water. Ellipsometry data were collected at temperatures 19°C < T < 32°C at ~1°C intervals at λ = 632.8 nm, with refractive index and thickness of the polymer layer simultaneously determined. Solution temperatures were measured using two separate thermistors in close proximity to the sample. The refractive index and thickness of the polymer layer were determined from Ψ and Δ using the Gaertner GEMP software following standard single wavelength ellipsometry calculations.[25, 26]

Single molecule fluorescence microscopy. Instrumentation and data acquisition parameters are described in detail elsewhere;[24] a brief description follows. The microscope is an objective-based total internal reflection fluorescence (TIRF) microscope, exhibiting a 100-200 nm depth of excitation and an effective pixel size of 267 nm x 267 nm with 60X magnification. Each frame was acquired with a 30 ms exposure, using frame transfer to eliminate delay time between frames. The acquisition protocol produced videos consisting of 1000 frames, which were obtained at 23°C and at 32°C in DI water. The temperature was controlled through a Peltier-controlled stage, described in detail elsewhere.[27] Briefly, a Peltier heating/cooling device with a custom build aluminum sample holder and a copper block where used to control and stabilize the temperature inside the sample holder. Temperature was monitored using a

thermocouple immersed in the solution of the sample holder. Single molecule tracking was carried out in a modified Matlab program[28, 29] developed specifically for SMT.[18, 30] Briefly, tracking consists of the linked tasks of identification, localization and trajectory reconstruction. Identification and localization were realized by fitting the spatial intensity profile of each suspect molecule to a 2-D Gaussian,

$$I(x,y) = I_0 \exp\left(-\frac{(x-x_0)^2}{2\sigma_x^2} - \frac{(y-y_0)^2}{2\sigma_y^2}\right) \quad (1)$$

from which the centroid (x_0, y_0) and the peak standard deviations (σ_x, σ_y) were obtained using a weighted linear least squares fit. The ratio of the peak height, I_0, to the standard deviation of the noise in the area adjacent to the peak was used to calculate the S/N and to determine if the peak qualified as a candidate single molecule. Localization was achieved by identifying the center of the 2D Gaussian, *i.e.* (x_0, y_0). If the S/N ratio is sufficient, then the centroid can always be localized to better precision than the diffraction limit.[29, 31] After every feature was identified in each frame, the frames were stacked in a movie and trajectories were linked together throughout the course of the movie.

Spatial resolution analysis. The limit of resolving motion in the images was first tested by simulating stationary fluorescent spots under varying S/N ratios and then applying the same tracking algorithms to the analysis of these simulated data. The S/N ratio for a given image was varied by first generating a Poisson distributed background at a mean intensity equivalent to that observed in the data, and then adding fluorescent spots modeled with a Gaussian function having a width given by the measured point-spread function (PSF) with Poisson distributed intensity noise. The apparent center locations (x_0,y_0) of these immobilized spots were then determined by the same tracking and localization algorithm as described above. A plot of the root-mean-square

variation (standard deviation) of these x_0,y_0 positions at different S/N ratios estimates the limit at which mobile and immobile fluorescent spots may be distinguished, which depends on the S/N ratio of the data. In order to test the predictions of this simulation, time-resolved images of immobilized R6G molecules deposited on a glass surface by dip coating from dilute ethanol solution[48,49] were acquired on the same microscope under the same conditions of molecular tracking experiments. The measured S/N ratio of these stationary single-molecule spots was 15, and the root-mean-square uncertainty in their positions was 16 nm. In order to generate higher S/N data to compare with the simulation results (and the higher S/N fluorescence from R6G diffusing in pNIPAAm), corresponding pixel intensities from multiple sequential frames from the same stack were added to generate a smaller series of frames. These co-added images had correspondingly greater molecular peak intensity and lower relative noise to provide higher S/N experimental data compare with the simulation results and the apparent motions of R6G in pNIPAAm.

Single molecule data analysis software and analysis. Confinement level functions in Matlab were modified to accept trajectory data from an existing tracking program and experimental protocol; this modified function is available online[24] and the rest of the program is available from the original authors.[32] Radius of gyration code was written in Matlab and is available online.[24] Gaussian and Lorentzian fits of the probability density functions for parameters from R_g evolution and confinement level calculations were carried out. The choice of model and number of peaks for each fit was determined by the best match to data in order to characterize peak position and width. No physical model is inferred from these fits.

Results and Discussion

Ellipsometry of hydrated pNIPAAm. Figure 1 shows the temperature response of a hydrated pNIPAAm brush on a silicon wafer, which exhibited 80 nm dry thickness. The ellipsometry results illustrate that the brush is thickest at 21°C and simultaneously reduces its thickness and increases its refractive index continuously until 32°C, with a ~20% decrease in free volume based on water content change. The gradual thickness transition observed here is typical for high density pNIPAAm brushes[33] as reported in the literature from surface plasmon resonance,[34] water contact angle,[35, 36] quartz crystal microbalanace,[37] neutron reflectometry,[38] sum frequency generation,[39] surface forces apparatus,[40] atomic force microscopy,[40] proton NMR,[41] neutron reflectometry,[4, 42] cyclic voltammetry,[43] and ellipsometry.[44] These measurements were used to determine data collection temperatures, 23°C and 32°C, for the SMT experiments, at which maximal differences in transport behavior might be expected.

Single molecule tracking. Four separate movies of R6G probes in the same pNIPAAm sample (unhydrated thickness 70nm) and the same field of view were analyzed, two each at 23°C and 32°C to assess the reproducibility of data collection. Trajectories are commonly limited in length by photobleaching and other processes that convert probes to long-lived dark states.[45-47] Because short trajectories are less useful for identifying differences between levels of confinement within a single track, only trajectories longer than 50 steps were used for further analysis, which resulted in 340 trajectories (29159 total steps) and 236 trajectories (18923 total steps) from the two movies at 23°C, and 1150 trajectories (99085 total steps), and 1238 trajectories (104565 total steps) from the movies at 32°C. The trajectories for R6G probes from SMT datasets at 23°C and 32°C are shown in Figs. 2 and 3, respectively. It is immediately evident that the partitioning coefficient of R6G into pNIPAAm is larger at 32°C than at 23°C, resulting in many more trajectories at the higher temperature. However, the initial concentration

is sufficiently small, even at 32°C, that it did not affect tracking results, meaning that there was negligible occurrence of probe-probe interactions, which could begin to occur when two probes occupy adjacent pixels in the same frame. However, even if probe molecules appear in adjacent pixels, they are hundreds of nanometers from each other within the x-y plane of the brush and can be many tens of nanometers from each other in the perpendicular z direction due to the film thickness. Therefore, remembering that the plots in Figs. 2 and 3 are compilations through all 1000 frames of a movie, using adjacent molecule-molecule appearances as a conservative criterion would still result in overestimating probe-probe events and these events were exceedingly rare. The probability that two molecules occupying the same pixel range is readily calculated with the Poisson distribution,

$$P(n) = \frac{\lambda^n e^{-\lambda}}{n!} \tag{2}$$

where λ is the probability of finding one molecule in a picture element and n is the number of events in a picture element, which can be determined from experimental parameters. The size of a frame (262144 pixels), size of a single molecule point spread function (9 pixels) and number of features per frame (~300) result in a 1% chance of observing a molecule in one 9 pixel range, λ. The Poisson distribution thus predicts there is less than 0.003% probability of observing two molecules in the same 9 pixel range.

Position and mobility of the probes are the main focus of the present study, therefore trajectories were used initially to quantify the movement of probe molecules such as space explored and time spent in localized areas. In addition, the metrics can be used to categorize probes into one of three classes as having: (a) small constant mobility (confined), (b) relatively large mobility (unconfined), and (c) those exhibiting one or more transitions between low and

high mobility states (intermittent confinement). These analysis methods are carried out with the aim of exploring free volume changes in the polymer films through the changes in probe mobility.

It is critical in this analysis to discriminate between low-mobility, confined diffusion of molecules within small domains in the polymer film, on the one hand, and strong interactions with fixed adsorption sites in the polymer that lead to molecules that are not moving on the time-scale of the observations, on the other. The question to be addressed is whether the measured motion of these low-mobility molecules exceeds the apparent motion of a dye molecule that is adsorbed to a surface and not moving. If the root-mean-square displacement of a R6G molecule during a confinement event clearly exceeds the apparent root-mean-square displacement of immobilized R6G molecules adsorbed to a surface, then the molecule is indeed diffusing within an entangled polymer domain. To test this question, both simulated and experimentally measured apparent root-mean-square displacements of stationary R6G molecules were compared at different S/N ratios, with excellent agreement between the experimental and simulated results; see Fig. 4. With higher S/N ratio, the resolution limits of discriminating moving versus immobile molecules improves, where experimental results find apparent root-mean-square displacements for adsorbed R6G at a glass-air interface of 16 nm, 9 nm and 3.5 nm for S/N ratios of 15, 25, and 50, respectively. The root-mean-square displacement of confined R6G molecules in pNIPAAm above the transition temperature is 60 nm for a S/N ratio of 30; see Fig. 4. At a S/N of 30, the resolution limit (root-mean-square apparent displacement of stationary molecules) is determined from simulation to be 6 nm. Therefore, the motion of confined molecules can be clearly distinguished from the apparent motion of stationary molecules, indicating that formation

of polymer entanglement domains is responsible for the confined regions of the trajectories, rather than adsorption to molecular-scale sites in the film.

This conclusion is further supported by comparing the ensemble-averaged diffusion coefficients of two different single molecules in pNIPAAm - R6G, $D_{avg} = 0.26\ \mu m^2\ s^{-1}$, and $DiIC_{18}$, $D_{avg} = 0.40\ \mu m^2\ s^{-1}$ (from previously published work[24]). The two probes are of similar size and charge, yet possess very different hydrophobic/hydrophilic characteristics. If chemically-specific probe-polymer chain interactions were a significant factor determining confined diffusion, the diffusion coefficients of these two probe populations would be expected to be significantly different. However, the two values differed by only ~1.5, suggesting that chemical interactions play a small role, if any, in determining the mobility of these molecules in pNIPAAm.

The diffusion coefficient, D, obtained from the slope of mean squared displacement, $\langle x^2 \rangle$, versus time delay, τ, is a commonly used metric when quantifying motion[11, 48] and useful as an initial analysis of the magnitude of mobility in these experiments. In addition, the shape of the $\langle x^2 \rangle$ *vs.* τ trace is an indication of the type of diffusion in the system- confined (sub-linear), Brownian (linear), or diffusion with flow (super-linear). However, individual probe variation and randomly intermittent behavior is lost in the averaging of the squared displacement. Thus, it is important to distinguish D values calculated for individual probes and those for ensemble averages over many probe molecules, and D values calculated for categorized segments. The ensemble-averaged diffusion coefficient (D_{ens}) calculated for the molecules studied in these experiments lies in the range $0.18\ \mu m^2\ s^{-1} < D_{ens} < 0.36\ \mu m^2\ s^{-1}$ independent of temperature. Since this cursory inspection of population-averaged diffusion coefficients produces the same

D_{ens} at 23°C and 32°C trajectories, despite the known LCST phase transition in the SRM, clearly a more thorough analysis is warranted.

Analysis of the temperature specific behavior of R6G probes was carried out using a suite of robust statistical tools available for comparison of SMT data.[24] Among the available tools, confinement level analysis[32, 49] and radius of gyration evolution[24] were found to be useful in distinguishing between pNIPAAm states and physical properties above and below the LCST. Confinement level calculations are carried out on a molecule-by-molecule basis in order to determine 'confined' and 'free' segments, *i.e.* portions or whole trajectories that exhibit higher and lower relative confinement relative to a well-defined threshold. Several metrics are obtained from these results, including the fraction of confined steps within the trajectory, α, the duration of confined and free portions of the trajectory, and the radii of free and confined zones. Once evaluated from SMT movies, these quantities can be compiled for all trajectories into histograms that convey the distribution of behaviors observed across the entire sample. The radius of gyration, R_g, of a trajectory describes the amount of space that the molecule explores during its movement, calculated as the root mean square distance from the trajectory's center of mass,

$$R_g = \sqrt{R_1^2 + R_2^2} \tag{3}$$

where R_1 and R_2 are the major and minor eigenvalues, respectively, of the radius of gyration tensor, $\boldsymbol{T}$. The tensor $\boldsymbol{T}$ is calculated from the x and y positions of the particle throughout its trajectory,

$$\hat{T} = \begin{pmatrix} \frac{1}{N}\sum_{j=1}^{N}\left(x_j - \langle x\rangle\right)^2 & \frac{1}{N}\sum_{j=1}^{N}\left(x_j - \langle x\rangle\right)\left(y_j - \langle y\rangle\right) \\ \frac{1}{N}\sum_{j=1}^{N}\left(x_j - \langle x\rangle\right)\left(y_j - \langle y\rangle\right) & \frac{1}{N}\sum_{j=1}^{N}\left(y_j - \langle y\rangle\right)^2 \end{pmatrix} \tag{4}$$

Thus, radius of gyration evolution quantifies the amount of space that a molecule explores over the course of the experiment. This value evolves over time for each molecule as motion is tracked and can be plotted *vs.* time in order to observe the progression. R_g evolution is especially useful in allowing the statistical outliers, for example molecules that exhibit multiple confined-to-mobile or mobile-to-confined transitions, to be identified in the presence of the ensemble-average behavior. In addition, all the values of R_g or the final R_g for each molecule can be plotted in a histogram to parse out measurable differences.

Confinement level calculations.[32, 49] Free and confined portions of each trajectory were compiled separately, from which individual probe molecule diffusion coefficients were determined from the mean squared displacement. Averaging over all segments placed in each category from all four movies yields $D_{confined} = 0.007\ \mu m^2\ s^{-1}$ and $D_{free} = 1.27\ \mu m^2\ s^{-1}$. The 'confined' diffusion segment can be considered immobile within the limits of the instrument and tracking limit given average 40 nm displacements from adsorbed R6G on glass, which yields a minimum diffusion coefficient of $0.013\ \mu m^2\ s^{-1}$ with 30 ms exposures. As with the ensemble averaged D, these values are helpful as a guide to the magnitude of the mobility corresponding to qualitatively distinct trajectory segments. In addition, they clearly define how much separation exist between the indicators for confined and free behavior observed overall in these samples. The next step beyond statistical description of confined and mobile segments examines the confinement level calculations of α, which show a consistent difference between temperatures above and below the LCST, as shown in Fig. 5. Statistical parameters from the Gaussian fits of the α distributions are compiled in Table 1. Consistent differences between high and low temperature fraction of confinement can be clearly observed in both the peak positions and widths of the α distributions. Both of the high temperature experiments evince a large fraction

of confined steps, while the 23°C data exhibit smaller peak α values. More strikingly, the low temperature distributions have a much longer tail at smaller α values, indicating a larger number of trajectories that exhibit a smaller fraction of confined steps. The usual increase in diffusion coefficient with temperature predicted by the Stokes-Einstein equation, corresponding to an increase in MSD under free diffusion conditions, stands in contrast to the larger degree of confinement at higher temperature seen in these data. This obvious, reproducible indication of the higher level of confinement at 32°C correlates well with the collapsed state of pNIPAAm, in spite of the increased thermal energy available to the probes.

Two additional metrics that can be extracted from confinement level analysis provide interesting insights into the differences between states of pNIPAAm above and below the LCST. Fig. 6(a) shows the duration of confined events, compiled as histograms of the confined portions of all trajectories. The 32°C traces (red) clearly show a long duration tail, giving a distribution that can be fit by a double Lorentzian function, while the 23°C traces (blue) show a single peak that fits a single Lorentzian. Furthermore, the fit parameters given in Table 2 confirm that the higher temperature distributions exhibit a second population of confined probe molecules that are immobile for ~ 4 times as long as the main part of the population. Additional insight into this phenomenon can be gleaned from the Lorentzian fits for the distributions of confined zone radii displayed in Fig. 6(b), which also exhibit systematic differences between $T > T_{LCST}$ and $T < T_{LCST}$. At 23°C the radii of confined zones in the two experiments peak at 54 nm with FWHM 70 nm and 43 nm with FWHM 31 nm, while at 32°C the distributions are sharper and smaller at 32 nm with FWHM 20 nm and 31 nm with FWHM 20 nm, a 34% average decrease at higher temperature.

When considered together, the confinement level analysis shows that in the 32°C state R6G probes in pNIPAAm: (i) exhibit a higher fraction of confined steps, (ii) are confined for longer periods of time, and (iii) are confined to smaller areas than in the 23°C state. In addition, the fact that two Lorentzian peaks best fit the duration of confined event histograms at 32°C suggests that there may be more than one distinct confinement mechanisms in pNIPAAm above the LCST.

Radius of gyration evolution. Radius of gyration evolution for two experiments, one at 23°C and the other at 32°C, are shown in Figs. 7(a) and 7(b), respectively. Only trajectories longer than 150 steps were included in these two plots in order that individual traces could be visually resolved. Differences between low and high temperature probe movement are readily apparent. Relatively immobile molecules, showing little increase in R_g over the course of the trajectory, and intermittent confinement behavior, as evidenced by consecutive increases and plateaus/decreases in R_g, are observable in both plots. However, the magnitude is clearly different above and below T_{LCST}. The difference in probe mobility between low and high temperature can be seen in the histogram of final R_g values for each molecule (trajectories longer than 50 steps) shown in Fig. 8. Clearly, a larger fraction of the trajectories end with higher final R_g values at 23°C than at 32°C, even though the most probable R_g values are near 50 nm, indicating confinement, at both temperatures. In addition, there is a small increase in the peak final R_g values going through T_{LCST}, as shown in Table 4. On average these values are larger for the low temperature pNIPAAm films (70 nm with FWHM 71 nm and 48 nm with FWHM 29 nm) than for those studied at high temperature (46 nm with FWHM 29 nm and 46 nm with FWHM 17 nm).

These results agree with those obtained from confinement level analysis, thereby augmenting the evidence for enhanced confinement in pNIPAAm at $T > T_{LCST}$. At 23°C the average radius of confinement of trajectory segments is 49 nm and the average final R_g is 59 nm, an increase of 20%. At 32°C the corresponding values are 32 nm and 46 nm, an increase of 44%. Therefore, single R6G molecule probes in PNIPAAm at 32°C explore less space and have larger jumps between confined zones than at 23°C.

Conclusion

A new method utilizing single molecule tracking to explore materials exhibiting temporally and spatially heterogeneous behavior has been applied to pNIPAAm, an archetypal SRM, at temperatures below and above its LCST, where it has been shown to exist in swelled and collapsed states, respectively. Several major conclusions can be drawn from a careful analysis utilizing confinement level and radius of gyration evolution to quantify the motion of R6G single molecule probes. First, probe behavior in the pNIPAAm films is best characterized by the degree of confinement that correlates with whether the film exhibits a swelled ($T < T_{LCST}$) or collapsed ($T > T_{LCST}$) morphology of the polymer and that behavior can be used to understand the different states of the brush. In addition, a combination of confinement level metrics - α, duration of confined events, and radius of confined zones - and radius of gyration evolution results can be used to illuminate the differing transport properties of hydrated pNIPAAm in swelled and collapsed states. Of particular note here is the consistent interpretation of probe motion in the collapsed state above the LCST as being confined to smaller areas, showing a higher fraction of confined segments and having a greater propensity to exhibit larger jumps between confined zones. Finally, this analysis of the non-Brownian (sub-diffusive) motion of

single probe molecules serves to highlight the benefits of tracking individual molecular probes as an approach to understanding the complex dynamics of network-based SRMs. We believe that this technique will find application to a wide range of soft materials in which nanometer-scale state changes are crucial to function, such as artificially engineered tissue, 3-D cell supports, extracellular matrix mimetics, and controlled drug delivery systems.

Acknowledgement

The work at Illinois and Notre Dame was supported by the National Science Foundation through a Graduate Fellowship (LCCE) and through grant NSF0807816. The work at Utah was supported by the U.S. Department of Energy under grant DE-FG03-93ER14333. A. Serge *et al.* generously shared their Matlab software and provided valuable discussion for confinement level computations.

Supplemental Information

The Matlab code used to calculate the radius of gyration evolution and the modified portion of confinement level calculations are available as Electronic Supplemental information online from a previous publication.[24]

References

1. M. W. Urban, *Polym. Rev.*, 2006, **46**, 329-339.
2. S. K. Ahn, R. M. Kasi, S. C. Kim, N. Sharma and Y. X. Zhou, *Soft Matter*, 2008, **4**, 1151-1157.

3. M. A. C. Stuart, W. T. S. Huck, J. Genzer, M. Muller, C. Ober, M. Stamm, G. B. Sukhorukov, I. Szleifer, V. V. Tsukruk, M. Urban, F. Winnik, S. Zauscher, I. Luzinov and S. Minko, *Nat. Mater.*, 2003, **9**, 101-113.

4. H. Yim, M. S. Kent, S. Mendez, G. P. Lopez, S. Satija and Y. Seo, *Macro.*, 2006, **39**, 3420-3426.

5. E. S. Gil and S. A. Hudson, *Prog. Polym. Sci.*, 2004, **29**, 1173-1222.

6. I. M. Khan and J. S. Harrison, eds., *Field Responsive Polymers. Electroresponsive, Photoresponsive, and Responsive Polymers in Chemistry and Biology. ACS Symposium Series 726* American Chemical Society, Washington, DC, 2000.

7. S. H. Gehrke, *Adv. Polym. Sci.*, 1993, **110**, 81-144.

8. R. H. Pelton and P. Chibante, *Coll. Surf.*, 1986, **20**, 247-256.

9. M. Kaholek, W. K. Lee, S. J. Ahn, H. W. Ma, K. C. Caster, B. LaMattina and S. Zauscher, *Chem. Mater.*, 2004, **16**, 3688-3696.

10. S. Chaterji, I. K. Kwon and K. Park, *Prog. Polym. Sci.*, 2007, **32**, 1083-1122.

11. A. Kusumi, Y. Sako and M. Yamamoto, *Biophys. J.*, 1993, **65**, 2021-2040.

12. A. Ishihara and K. Jacobson, *Biophys. J.*, 1993, **65**, 1754-1755.

13. R. N. Ghosh and W. W. Webb, *Biophys. J.*, 1994, **66**, 1301-1318.

14. U. Kubitscheck, P. Wedekind and R. Peters, *Biophys. J.*, 1994, **67**, 948-956.

15. M. J. Saxton, *Biophys. J.*, 1995, **69**, 389-398.

16. R. J. Cherry, K. M. Wilson, K. Triantafilou, P. O'Toole, I. E. G. Morrison, P. R. Smith and N. Fernandez, *J. Cell Biol.*, 1998, **140**, 71-79.

17. R. Simson, E. D. Sheets and K. Jacobson, *Biophys. J.*, 1995, **69**, 989-993.

18. J. C. Crocker and D. G. Grier, *J. Colloid Interface Sci.*, 1996, **179**, 298-310.

19. S. Ito, T. Kusumi, S. Takeiac and H. Miyasaka, *Chem. Commun.*, 2009, **41**, 6165-6167.

20. K. S. McCain, D. C. Hanley and J. M. Harris, *Analyt. Chem.*, 2003, **75**, 4351-4359.

21. M. J. Saxton and K. Jacobson, *Annu. Rev. Biophys. Biomol. Struct.*, 1997, **26**, 373-399.

22. R. M. Dickson, D. J. Norris, Y. L. Tzeng and W. E. Moerner, *Science*, 1996, **274**, 966-969.

23. I. Lokuge, X. Wang and P. W. Bohn, *Langmuir*, 2007, **23**, 305-311.

24. L. C. C. Elliott, M. Barhoum, J. M. Harris and P. W. Bohn, *Phys. Chem. Chem. Phys.*, 2011, DOI: 10.1039/c1030cp01805h.

25. H. G. Tompkins, *A User's Guide to Ellipsometry*, Academic Press, Inc., San Diego, CA, 1993.

26. H. G. Tompkins and E. A. Irene, *Handbook of Ellipsometry*, William Andrew Publishing, Norwich, NY, 2005.

27. C. B. Fox, G. A. Myers and J. M. Harris, *Appl. Spectrosc.*, 2007, **61**, 465-469.

28. S. Anthony, L. F. Zhang and S. Granick, *Langmuir*, 2006, **22**, 5266-5272.

29. S. M. Anthony and S. Granick, *Langmuir*, 2009, **25**, 8152-8160.

30. E. R. Weeks, J. C. Crocker, A. C. Levitt, A. Schofield and D. A. Weitz, *Science*, 2000, **287**, 627-631.

31. X. H. Qu, D. Wu, L. Mets and N. F. Scherer, *Proc. Natl. Acad. Sci. USA*, 2004, **101**, 11298-11303.

32. A. Serge, N. Bertaux, H. Rigneault and D. Marguet, *Nature Methods*, 2008, **5**, 687-694.

33. R. Barbey, L. Lavanant, D. Paripovic, N. Schuwer, C. Sugnaux, S. Tugulu and H. A. Klok, *Chem. Rev.*, 2009, **109**, 5437-5527.

34. S. Balamurugan, S. Mendez, S. S. Balamurugan, M. J. O'Brien and G. P. Lopez, *Langmuir*, 2003, **19**, 2545-2549.

35. Q. He, A. Kuller, M. Grunze and J. B. Li, *Langmuir*, 2007, **23**, 3981-3987.

36. T. L. Sun, G. J. Wang, L. Feng, B. Q. Liu, Y. M. Ma, L. Jiang and D. B. Zhu, *Angew. Chem. Int. Ed.*, 2004, **43**, 357-360.

37. M. Annaka, C. Yahiro, K. Nagase, A. Kikuchi and T. Okano, *Polymer*, 2007, **48**, 5713-5720.

38. N. Ishida and S. Biggs, *Macro.*, 2010, **43**, 7269-7276.

39. V. Kurz, M. Grunze and P. Koelsch, *Chemphyschem*, 2010, **11**, 1425-1429.

40. I. B. Malham and L. Bureau, *Langmuir*, 2009, **26**, 4762-4768.

41. Q. S. Wei, J. Ji and J. C. Shen, *Macromol. Rapid Commun.*, 2008, **29**, 645-650.

42. A. Vidyasagar, J. Majewski and R. Toomey, *Macro.*, 2008, **41**, 919-924.

43. Z. Z. Yin, J. J. Zhang, L. P. Jiang and J. J. Zhu, *J. Phys. Chem. C*, 2009, **113**, 16104-16109.

44. H. Tu, C. E. Heitzman and P. V. Braun, *Langmuir*, 2004, **20**, 8313-8320.

45. L. A. Deschenes and D. A. V. Bout, *Chem. Phys. Lett.*, 2002, **365**, 387-395.

46. J. Schuster, J. Brabandt and C. von Borczyskowski, *J. Lumin.*, 2007, **127**, 224-229.

47. M. A. van Dijk, L. C. Kapitein, J. van Mameren, C. F. Schmidt and E. J. G. Peterman, *J. Phys. Chem. B*, 2004, **108**, 6479-6484.

48. K. Ritchie, X. Y. Shan, J. Kondo, K. Iwasawa, T. Fujiwara and A. Kusumi, *Biophys. J.*, 2005, **88**, 2266-2277.

49. S. de Keijzer, A. Serge, F. van Hemert, P. H. M. Lommerse, G. E. M. Lamers, H. P. Spaink, T. Schmidt and B. E. Snaar-Jagalska, *J. Cell Sci.*, 2008, **121**, 1750-1757.

Figures and Tables

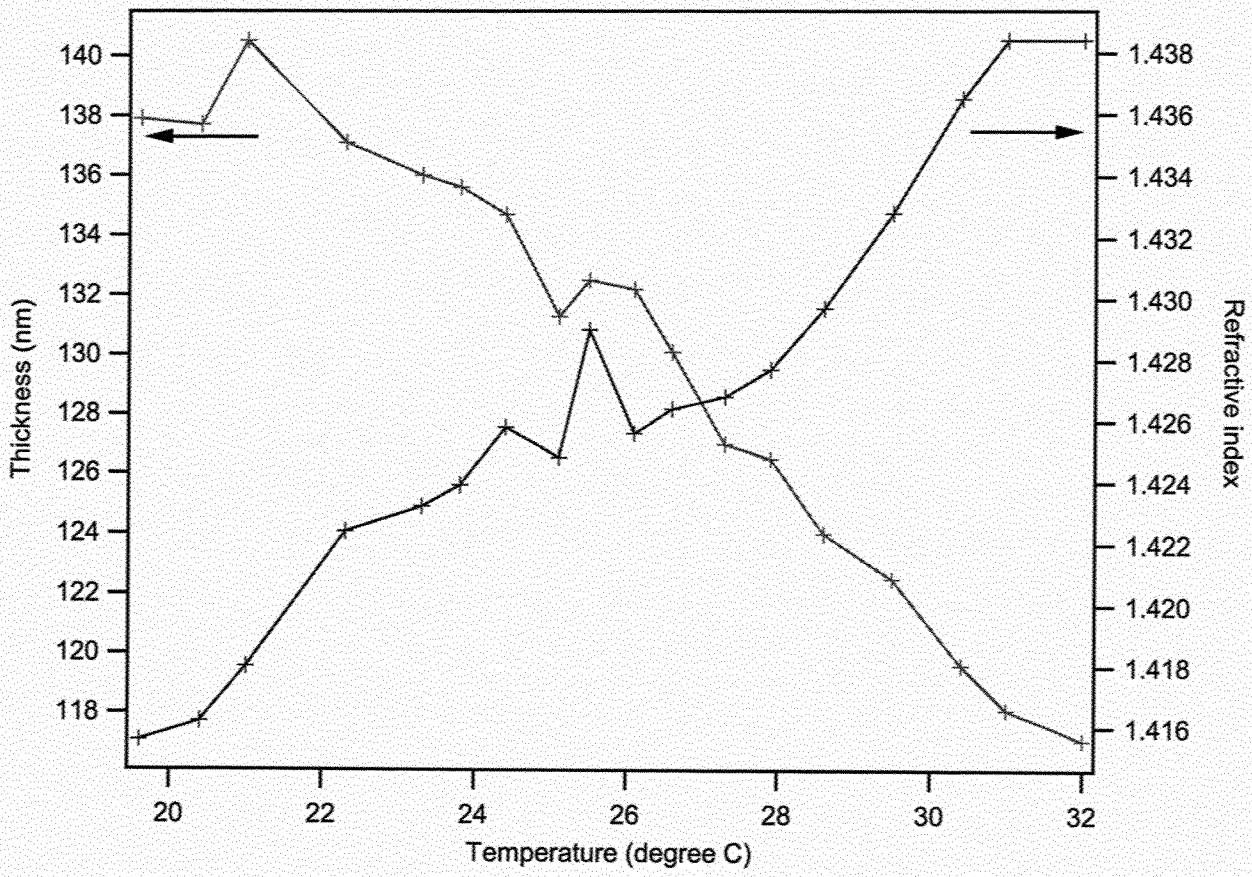

Figure 1. Ellipsometric measurements of thickness (red) and refractive index (blue) as a function of temperature for hydrated pNIPAAm synthesized on Si with 5 min reaction time. Film displayed 80 nm dry thickness.

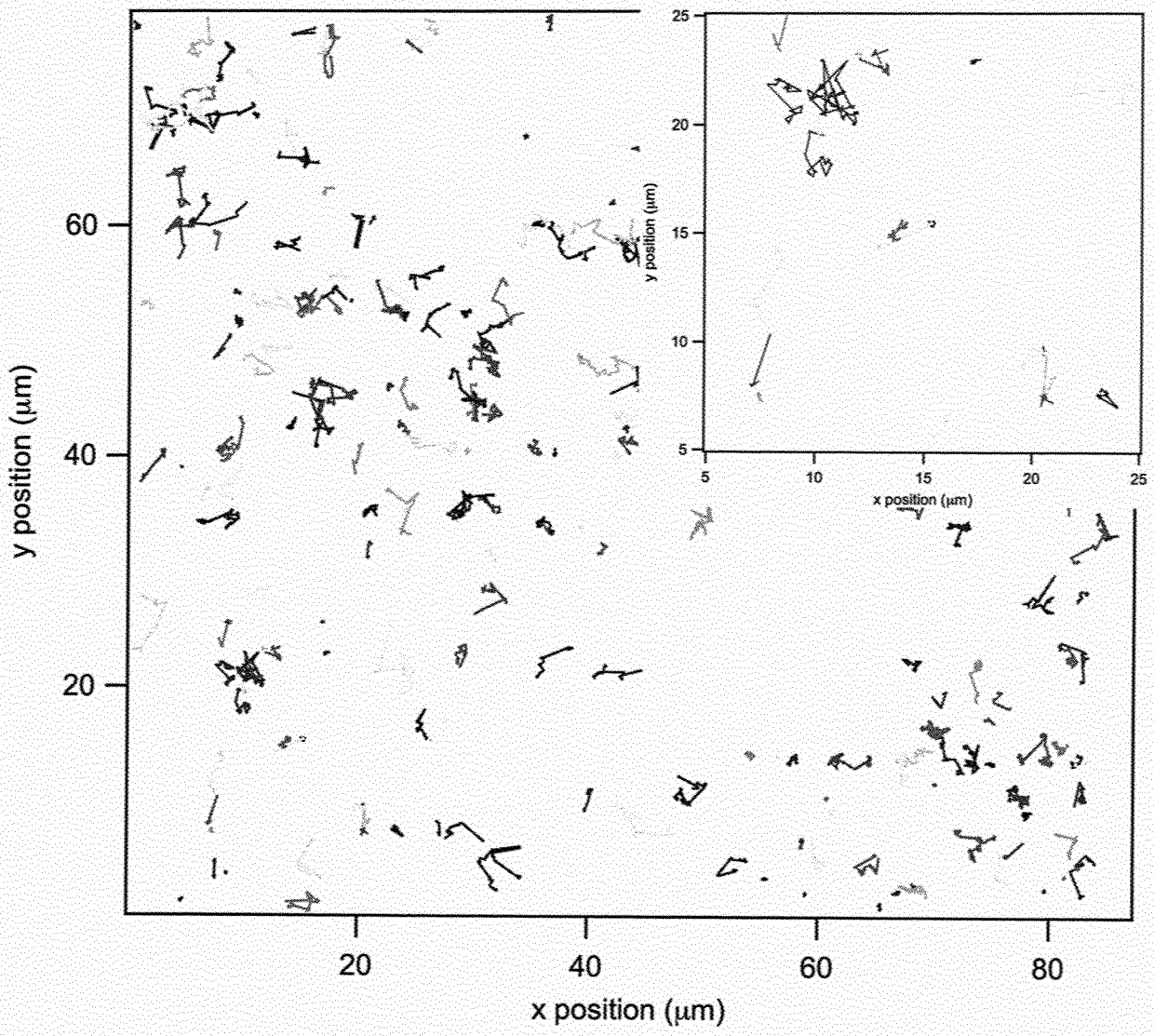

Figure 2. Reconstructed SMT trajectories longer than 50 frames for R6G in pNIPAAm on glass at 23°C (polymer brush in expanded state); (*Inset*) 20 μm x 20 μm expanded view. Different colors are used for clarity only.

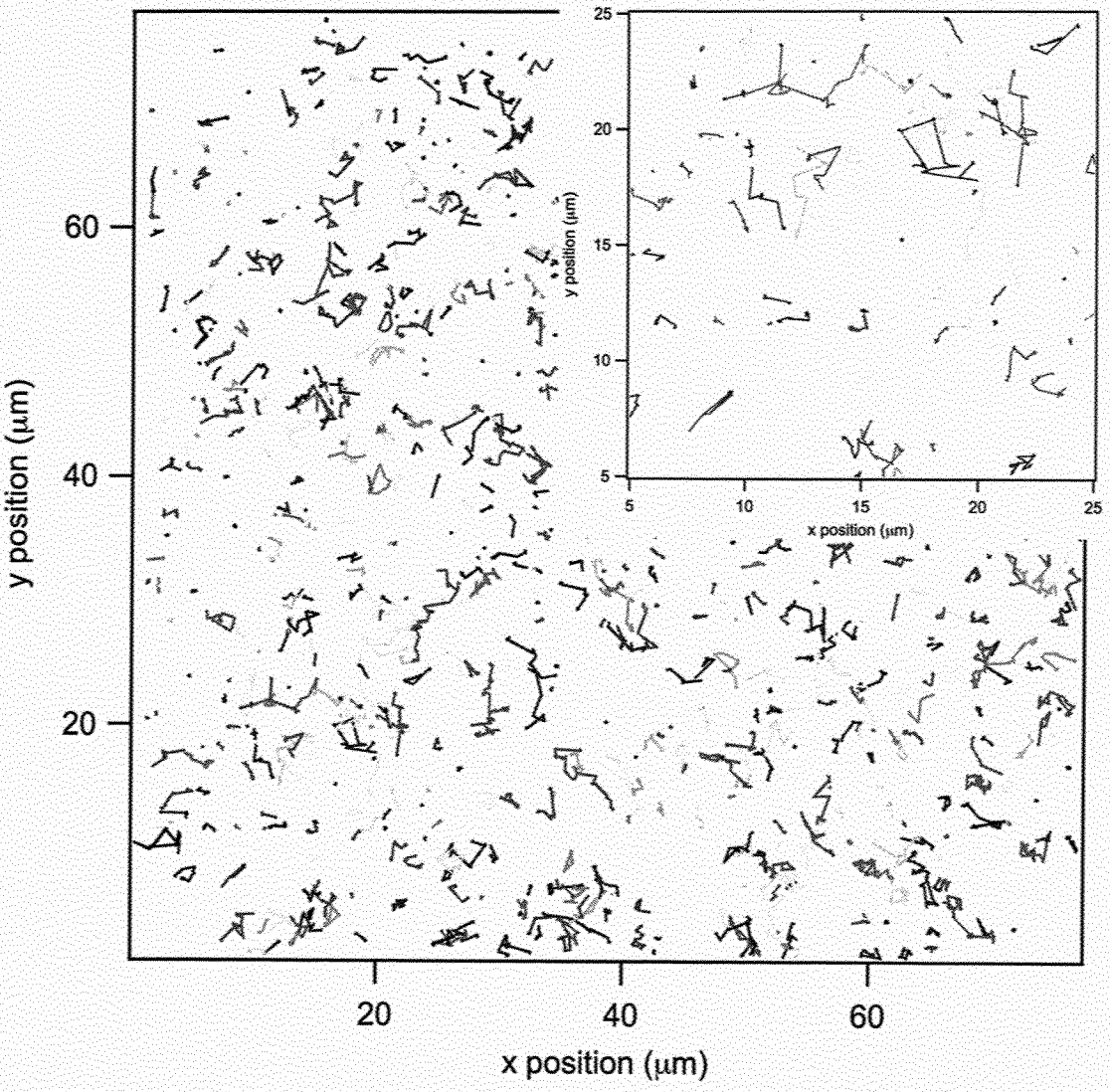

Figure 3. Reconstructed SMT trajectories longer than 50 frames for R6G in pNIPAAm on glass at 32°C (polymer brush in collapsed state); (*Inset*) 20 μm x 20 μm expanded view. Different colors are used for clarity only.

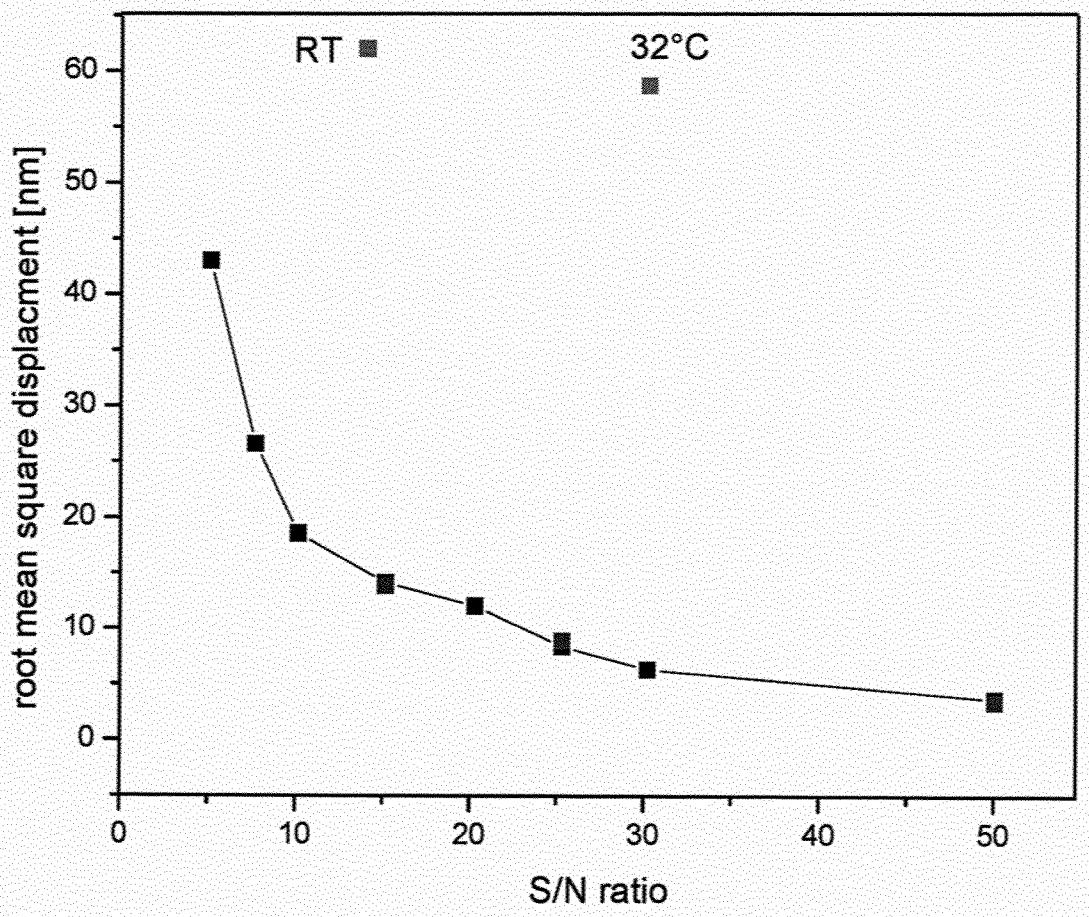

Figure 4. Root mean square displacement for R6G molecules adsorbed to a surface site as a function of the S/N ratio of the single molecule fluorescent image for both simulated (black) and experimental (blue) data. Red squares correspond to the experimentally determined rms displacement and S/N for confined R6G molecules in pNIPAAm both below (RT ~ 25 °C) and above the LCST, as noted.

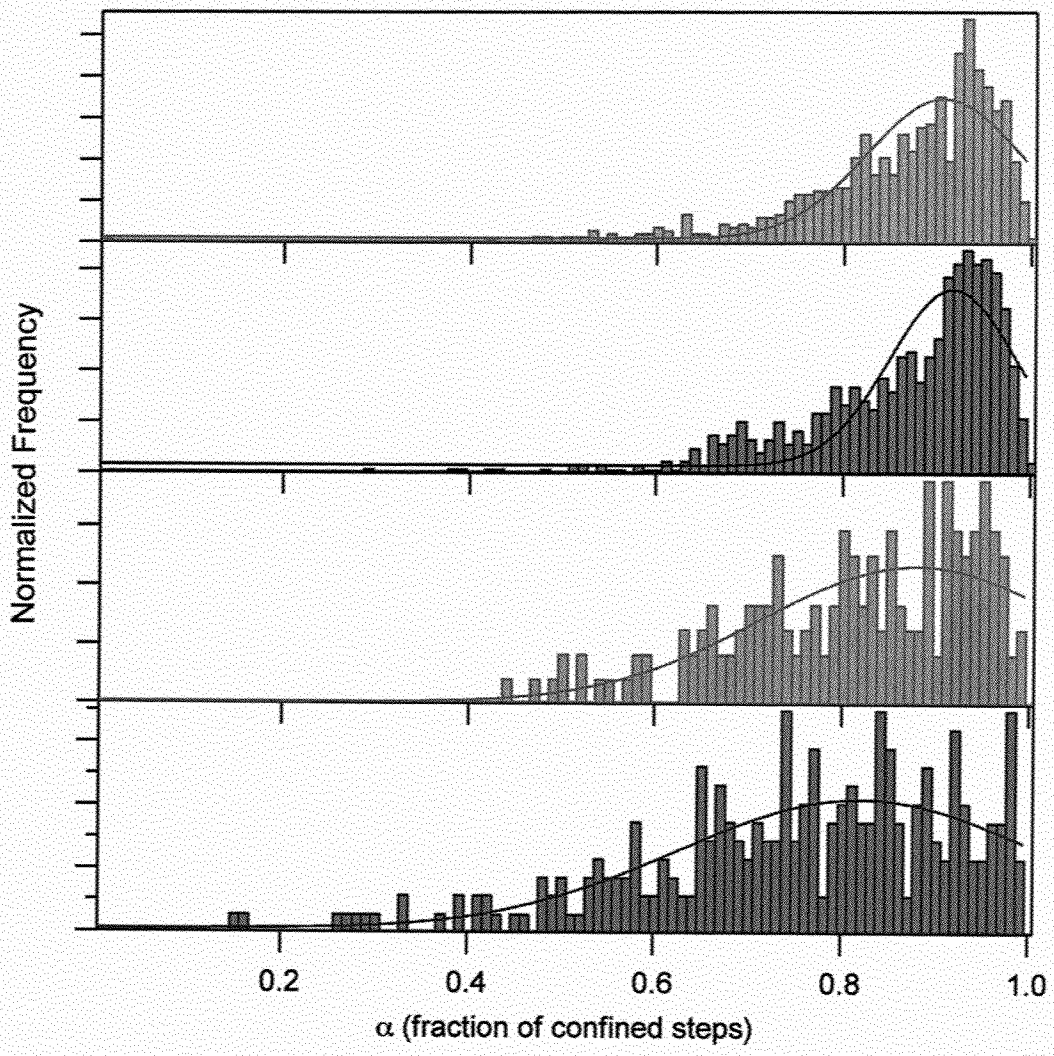

Figure 5. Confinement level analysis results for two separate samples of R6G probes in the same pNIPAAm sample on glass at 23°C (dark red, light red) and 32°C (dark blue, light blue). Solid lines are Gaussian curve fits with peak and width parameters given in Table 1.

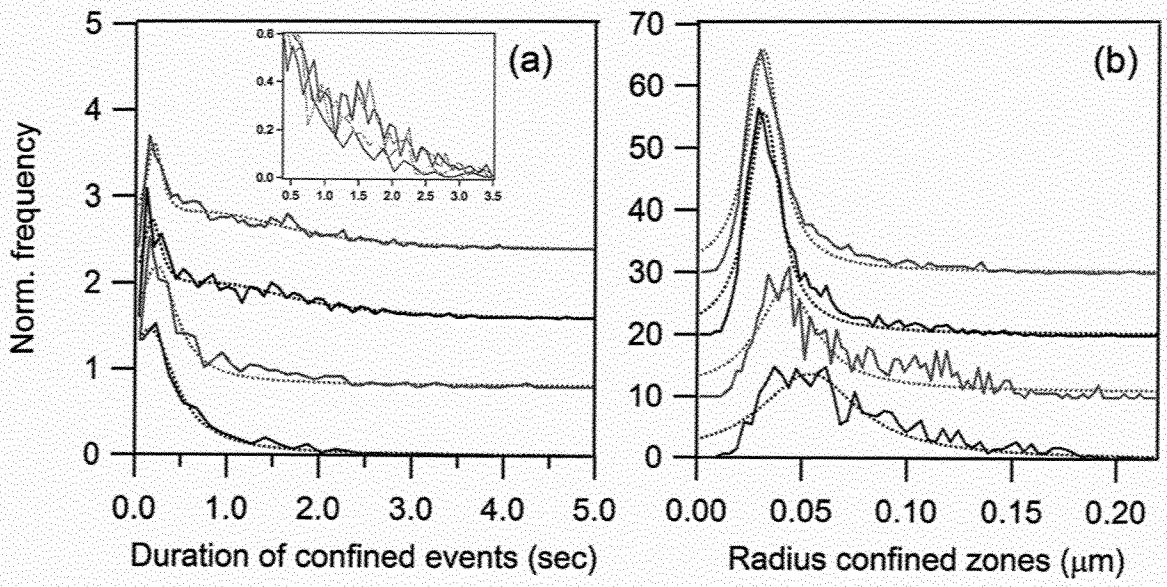

Figure 6. Confinement level analysis for R6G in pNIPAAm at 23°C (dark red, light red) and 32°C (dark blue, light blue), two trials each. Traces are offset for clarity and the inset emphasizes the difference between the tail at 23°C and 32°C. (a) Normalized histograms of the duration of confined events, with fits (dashed lines) for single (23°C) and double (32°C) Lorentzian functions. Fit parameters are given in Table 2. (b) Distribution of the radius of confined zones. Single Lorentzian functions (dashed lines) are fit to these distributions, with peak and width parameters given in Table 3.

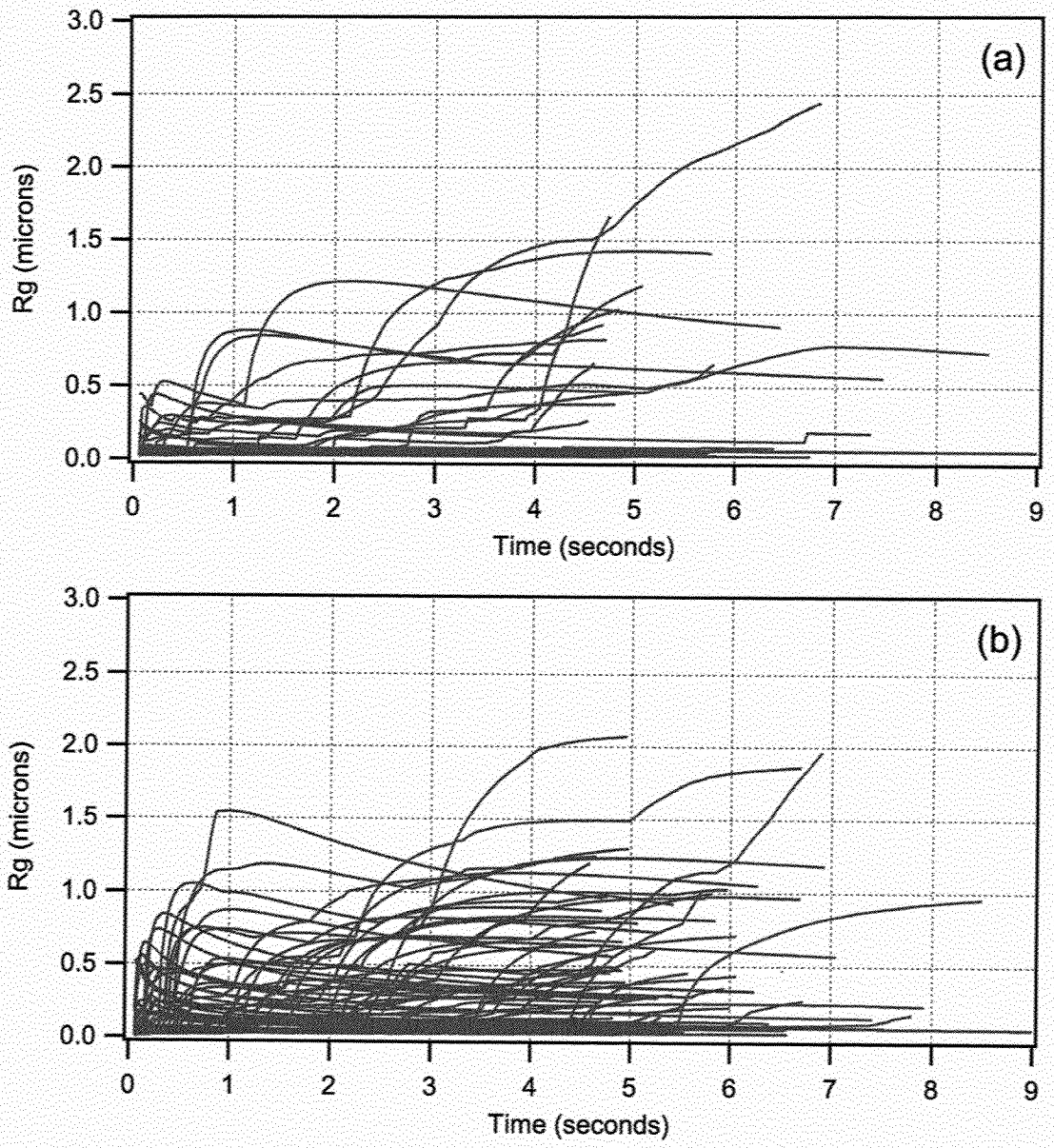

Figure 7. Radius of gyration evolution for trajectories at 23°C (a) and 32°C (b) of R6G in pNIPAAm on glass. Only trajectories longer than 150 steps only are included.

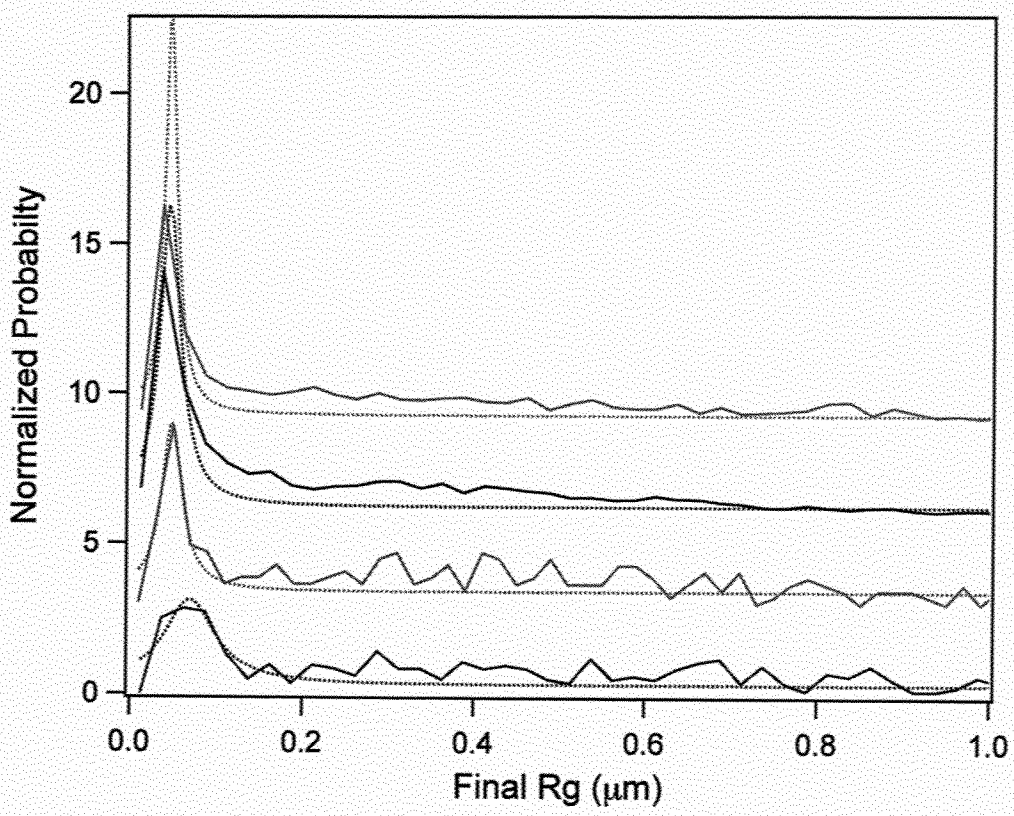

Figure 8. Histograms of the final R_g value for each molecule in SMT movies 23°C (dark and light red) and 32°C (dark and light blue). The traces are offset for clarity. Peaks and FWHM from Lorentzian fits to the experimental histograms are given in Table 4.

Table 1. Gaussian fit parameters for experimental confinement level histograms in Figure 4.

Temperature	Width	Peak
32°C (#2)	0.12	0.91
32°C (#1)	0.10	0.92
23°C (#2)	0.24	0.88
23°C (#1)	0.27	0.82

Table 2. Lorentzian fit parameters for confined event duration histograms in Figure 5(a).

Temperature	Peak A (sec)	Width A (sec)	Peak B (sec)	Width B (sec)
32°C (#2)	0.20	0.06	0.82	0.31
32°C (#1)	0.18	0.01	0.91	2.04
23°C (#2)	0.23	0.52	--	--
23°C (#1)	0.16	0.68	--	--

Table 3. Lorentzian fit parameters for confined zone radius histograms in Figure 5(b).

Temperature	Peak (nm)	Width (nm)
32°C (#2)	31	20
32°C (#1)	32	20
23°C (#2)	43	31
23°C (#1)	54	70

Table 4. Lorentzian fit parameters for final R_g histograms in Figure 7.

Temperature	Peak (nm)	Width (nm)
32°C (#2)	46	17
32°C (#1)	46	29
23°C (#2)	48	29
23°C (#1)	70	71